NURETH14-599

PROGRESS IN THE PREDICTION OF NON-UNITY PRANDTL-NUMBER TURBULENT FLOWS USING TransAT

D. Lakehal, J. Panyasantisuk, D. Caviezel, M. Labois and C. Narayanan ASCOMP GmbH, Zurich, Switzerland lakehal@ascomp.ch; Lakehal@ascomp.ch

Abstract

We report LES results of the flow and convective heat transfer in a heated channel at a wall shear Reynolds number of $Re_{\tau} = 150$ and 171. The results are compared with available DNS data for various Prandtl number fluids (Pr = 0.1-10). In order to deal with non-unity Pr fluid flows, we have extended the variant of the Dynamic sub-grid scale (SGS) model of Germano proposed by Lilly [1] to the thermal field, whereby the motion of the unresolved fluid flow and thermal structures is dictated by the resolved thermal-flow field. The base LES strategy as built in the code TransAT has been first validated for a practical case: the thermal-flow in a T junction, showing time-averaged results with excellent agreement with the experiment. The extended SGS model to the thermal field delivers results in line with the DNS data of a heated channel flow, and reveals that the turbulent Prandtl number cannot be fixed in an *ad-hoc* manner, and is clearly dependent on both the fluid and flow properties.

Introduction

Non-unity Prandtl number flows are clearly out of reach of traditional RANS modeling approaches, in which the rate of mechanical production to thermal production is assumed to adhere to the Reynolds analogy. There are various incentives to further develop modeling strategies transcending Reynolds analogy, both within the RANS and LES contexts. This is particularly true for thermal-hydraulics applications involving heavy liquid metals [2], and Supercritical Pressure Water [3]. There exist various types of analytical models linking the turbulent Prandtl number to the molecular one [4, 5], which could be used in combination with linear Eddy-Viscosity models (EVM). But none of these was really assessed against DNS.

Past experience shows that the EVM approaches need to be replaced with more sophisticated variants; including anisotropy of dynamics and thermal turbulent stresses and fluxes (the so-called EASM for turbulent stresses, and GGDH and WET for turbulent heat fluxes [6]). Further, it seems that even with these sophisticated approaches, non-unity Prandtl-number fluid flows will not be well predicted, in particular in situations involving strong buoyancy effects, in which case resort is made to the so-called k- ε - θ - ε - θ model [7], in which two extra transport equations are solved for the temperature variance, θ - θ -, and its rate of dissipation, ε _{θ}. The second strategy consists in resorting to LES, short for Large-Eddy Simulation. Here the super-grid scales (SG) are directly solved while the smallest ones (called Sub-Grid Scales; SGS) are modeled. Both modeling strategies are available in the CMFD code TransAT [8].

This paper presents the SGS modeling strategy used for the purpose. This is based on the dynamic approach [1] (DSM), extended to the thermal field [9, 10] such that the motion of the unresolved thermal structures is dictated by the resolved thermal-flow field. The basic LES strategy of TransAT is first validated for the well-documented thermal-flow in a T junction [11].

1. Model formulation

1.1 The filtered equations

The filtered Navier-Stokes equations governing incompressible single-phase fluid flow with heat transfer take the form:

$$\nabla \cdot \overrightarrow{\mathbf{u}} = 0$$

$$\frac{\partial}{\partial t} \left(\rho \overrightarrow{u_i} \right) + \nabla \cdot \left(\rho \overrightarrow{u_i} \overrightarrow{u_j} \right) = -\nabla \overrightarrow{p} + \nabla \cdot \left(\overrightarrow{\sigma} - \tau \right) + F_b + F_c$$

$$\frac{\partial \left(\rho C p \overrightarrow{T} \right)}{\partial t} + \nabla \left(\rho C p \overrightarrow{T} \overrightarrow{u_j} \right) = \nabla \left(\lambda \nabla \overrightarrow{T} \right) - C p \nabla q'' + Q'''$$
(1)

where $\bf u$ stands for the fluid velocity and p for the pressure, ρ is the density, μ is the viscosity, λ is the thermal conductivity, C_p is the heat capacity, and Q''' is the volumetric heat source. The source terms in the RHS of the momentum equation represents the body force, F_b , and the convolution-induced terms for non-equidistant and body fitted grids, F_c . Further, the filtered LES equations introduce the so-called SGS stress tensor and turbulent heat flux defined as:

$$\tau_{ij} \equiv \overline{\rho} \left(\overline{u_i u_j} - \overline{u_i} \, \overline{u_j} \right); \quad q_j^{"} \equiv \overline{\rho} \left(\overline{T u_j} - \overline{T} \, \overline{u_j} \right) \tag{2}$$

Only the deviatoric part of the SGS stress tensor is to be modeled using a statistical approach similar to RANS; and the same is true of the turbulent heat flux. This way, turbulent scales larger than the grid size are directly solved, whereas sub- or SGS scales are modeled. The LES equations and sub-grid scale models are now well known; details can be found in [1, 9].

1.2 SGS modeling: the Dynamic approach (DSM)

LES is based on the concept of filtering the flow field by means of a convolution product. The specific super-grid part of the flow with its turbulent fluctuating content is directly predicted whereas the sub-grid scale (SGS) part is modeled, assuming that these scales are more homogeneous and universal in behavior. For turbulent flows featuring a clear inertial subrange the modeling of the SGS terms in the statistical sense could thus safely borrow ideas from the RANS context, in particular use of the zero-equation model to mimic the momentum diffusive effects on the resolved field. Use is generally made of the Eddy Viscosity Concept (known as the Boussinesq approach), linking linearly the SGS eddy viscosity and thermal diffusivity to the gradients of the filtered velocity and temperature, respectively:

$$\tau_{ij} = -2\mu_{sgs}\overline{S_{ij}} + \frac{1}{3}\delta_{ij}\tau_{ll}; \quad \mu_{sgs} = (Cs\Delta)^{2}\overline{\rho}\left|\overline{S}\right|^{2}$$

$$q_{j}^{"} = -\alpha_{\theta}\frac{\partial\overline{T}}{\partial x_{i}}; \quad \alpha_{\theta} = \frac{\mu_{sgs}}{Pr_{t}}$$
(3)

The closure for the eddy viscosity above follows in general the Smagorinsky kernel model, linking the eddy viscosity to the square of a length scale and a time scale (the inverse of the second invariant of the resolved rate of deformation tensor S_{ij}). The model constant (C_s) is either fixed or made dependent on the flow; this later option is precisely the spirit of the dynamic model. A damping function is often introduced for the model constant Cs to accommodate the asymptotic behavior of near-wall turbulence. Similarly, the same strategy could be used to close the turbulent SGS heat flux, where the thermal diffusivity could be determined either based on the resolved thermal-flow field, or alternatively based on the eddy viscosity (defined dynamically) and a fixed. Using the first alternative means that the turbulent Prandtl number is not imposed but is a result of the model. The advantage of DSM compared the base model is that the model constant Cs may be negative, which does not exclude possible backscatter of energy, it returns the proper asymptotic behavior of the stresses near the wall with damping as required by the base model, and vanishes in laminar flow without ad-hoc intermittency functions [9].

The DSM approach requires though a two-level filtering, in contrast to simple Smagorinsky model, in which filtering is actually implicit, based on the grid only. The approach is based on the application of a second larger filter ($\overline{\Delta} = 2\Delta$) on top of the filtered equations (1). Without presenting the details of the model, the dynamic length scale for both the thermal and flow field are determined as follows [9] (using the least-square approach):

$$(C_{s}\Delta)^{2} = -\frac{1}{2} \frac{\langle L_{ij} \rangle \langle M_{ij} \rangle}{\langle M_{ij} \rangle}; \quad (C_{\theta}\Delta)^{2} = -\frac{\langle L_{j} \rangle^{\theta} \langle M_{j} \rangle^{\theta}}{\langle M_{j} \rangle^{\theta} \langle M_{j} \rangle^{\theta}}$$

$$\langle L_{ij} \rangle = -2(C_{s}\Delta)^{2} \left[\left(\frac{\overline{\Delta}}{\Delta} \right)^{2} \left| \overline{\overline{S}} \right| \overline{\overline{S_{ij}}} - \overline{|\overline{S}|} \overline{\overline{S_{ij}}} \right]; \quad \langle M_{ij} \rangle = \left| \overline{\overline{S}} \right| \overline{\overline{S_{ij}}} - \overline{|\overline{S}|} \overline{\overline{S_{ij}}}$$

$$\langle L_{j} \rangle^{\theta} = -(C_{\theta}\Delta)^{2} \left[\left(\frac{\overline{\Delta}}{\Delta} \right)^{2} \left| \overline{\overline{S}} \right| \frac{\partial \overline{\overline{T}}}{\partial x_{j}} - \overline{|\overline{S}|} \frac{\partial \overline{\overline{T}}}{\partial x_{j}} \right]; \quad \langle M_{j} \rangle^{\theta} = \left| \overline{\overline{S}} \right| \frac{\partial \overline{\overline{T}}}{\partial x_{j}} - \overline{|\overline{S}|} \frac{\partial \overline{\overline{T}}}{\partial x_{j}}$$

where < . > denotes plane-averaging in flows with a clear homogeneous direction, e.g. channel flow. Using these two length scales to determine the SGS eddy viscosity and diffusivity separately helps derive the dynamic expression for the turbulent Prandtl number [9, 10]. The advantage of the DSM approach here is its capacity to sensitize the eddy diffusivity to the resolved thermal-flow field. This may sound somewhat conflicting with the analytical models linking the turbulent Prandtl number to the molecular one, e.g. [4, 5]. Be it as it may, using the DSM approach will help shed light on various issues: whether the turbulent Prandtl number Pr_t is truly independent of Pr only for Pr < 0.1, and whether the sharp transition for Pr_t is at Pr = 0.01, as stipulated from experimental observations (i.e. Pr_t suddenly increases for Pr < 0.01, otherwise it remains in the range 2-4). Our intention is to use the model and calibrate analytical approaches.

2. The numerical approach in TransAT

The CFD/CMFD code TransAT© developed at ASCOMP [8] is a multi-physics, finite-volume code based on solving multi-fluid Navier-Stokes equations. The code uses structured meshes, though allowing for multiple blocks to be set together. MPI parallel based algorithm is used in connection with multi-blocking. The grid arrangement is collocated and can thus handle more easily curvilinear skewed grids. The solver is pressure based (Projection Type), corrected using the Karki-Patankar technique for compressible flows. High-order time marching and convection schemes can be employed; up to third order Monotone schemes in space. Multiphase flows can be tackled using (1) interface tracking techniques for both laminar and turbulent flows (Level Set, VOF with interface reconstruction, and Phase Field), (2) phase-averaged homogeneous mixture model (Algebraic Slip), and (3) Lagrangian particle tracking (one-to-four way coupling).

3. Thermal flow in the Vattenfall T-junction

3.1 Test facility description

Obviously this flow does not require a specific model for turbulent Prandtl number, and as such it only serves the purpose of validation of the base LES approach as built in the code. The tests were carried out at the Älvkarleby Laboratory, Vattenfall R&D; the flow conditions are documented in [11]. The test rig, illustrated in Fig. 1, was designed to obtain well-defined inlet boundary conditions. The setup consists of a horizontal pipe with inner diameter 140 mm for the cold water flow (Q2), and a vertically oriented pipe with inner diameter 100 mm for the hot water flow (Q1). The hot water pipe is attached to the upper side of the horizontal cold water pipe. The length of the pipes upstream of the T-junction is more than 80 diameters for the cold water inlet, and approximately 20 diameters for the hot water inlet.

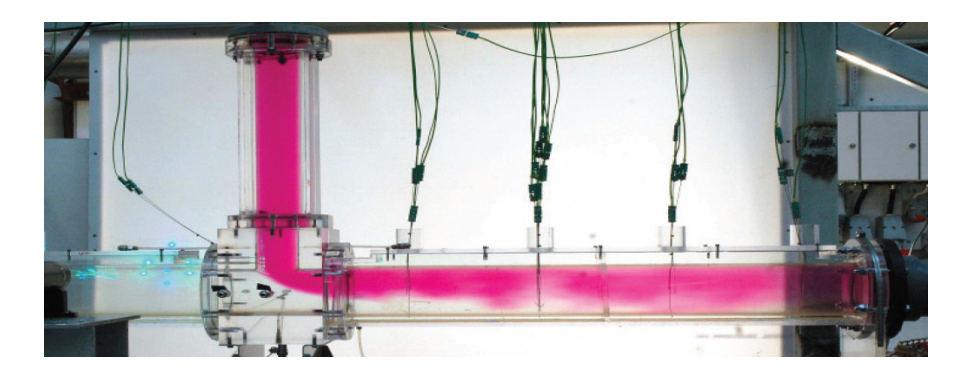


Figure 1: Flow visualization test in the Vattenfall T-junction experiment [11]

A stagnation chamber with flow improving devices (tube bundles and perforated plates) is located at the entrance to each of the two inlet pipes. The temperature fluctuations near the walls were measured by Westin et al. [11], with thermocouples located approximately 1 mm from the pipe wall. Two different types of thermocouples were used, with an estimated frequency response of 30 Hz and 45 Hz respectively. Velocity profiles were measured with two-component LDV in each inlet pipe as well as in cross-sections located 2.6 and 6.6 diameters downstream of

the T-junction. The mixing process has also been studied with single-point LIF at isothermal conditions. The pipes near the T-junction were made of Plexiglas tubes surrounded by rectangular boxes filled with water in order to reduce the diffraction when the laser beams pass the pipe walls.

The tests were carried out with a constant flow ratio Q2/Q1=1.5, and a temperature difference between the hot and cold water of 17°C (hot water temperature T1=36°C). The Reynolds number in both inlet pipes were approximately 8E5 for the considered test case with bulk velocities of approximately 0.77 m/s in the hot leg and 0.58 m/s in the cold leg (corresponding to Q1=6 l/s and Q2=9 l/s). The LDV-measurements in the cold water pipe just upstream of the T-junction showed mean velocity and turbulence profiles in good agreement with experimental data on fully developed pipe flow at similar Reynolds numbers. The length of the hot water inlet pipe was too short (20 diameters) to obtain fully developed flow conditions, but the inlet velocity profiles were measured in order to obtain inlet boundary conditions for the simulations. Therefore for the CFD investigations the measured velocity profiles were used for both inlet cross-sections.

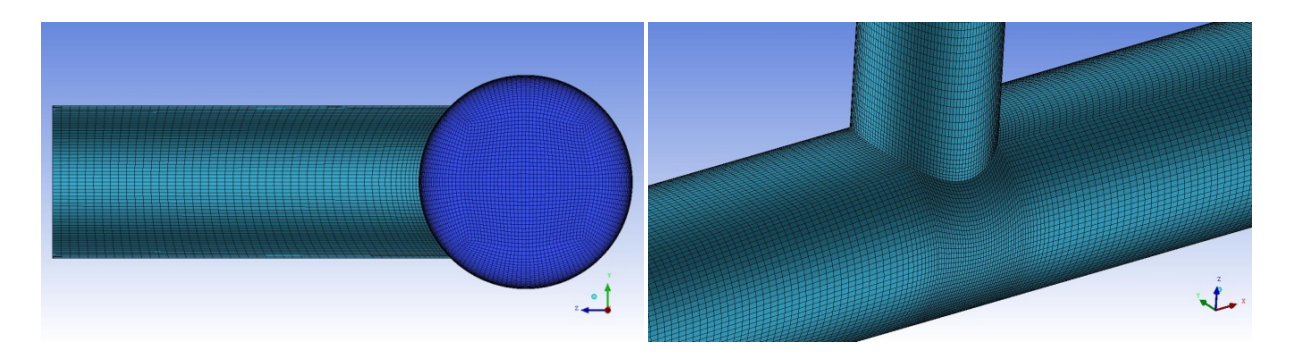


Figure 2: Computational multi-block domain and BFC grid

3.2 Problem setup

The filtered transport equations were solved using the WALE SGS model [12]. A body-fitted mesh was used consisting of 2.49 Mio cells. The inlets were deliberately reduced, and thus the domain starts at x = -0.42 m for the cold inlet, and z = +0.31 m for the hot inlet. The exit plane was located at x = 2.24 m. The grid distribution was carefully controlled, with a minimum size of 1.9 mm and an aspect ratio of 3 in the x direction, and 0.15 mm in y- and z-directions, respectively. The wall-neighboring cell of 0.15mm resulted in a y+ value falling in the range 6 to 9, justifying the need to use wall functions. Water properties were taken at 25°C. For the inlet fluid flow conditions, synthetic turbulent inflow profiles were generated. An adaptive time-stepping strategy (using explicit time marching) has been chosen, ensuring that 0.1 < CFL < 0.3. This led to an average time step of 9.5e-5 s varying in the course of the simulation.

The flow reaches a steady state after about 3.5 s, after which time and space averaging of the flow has been performed, typically between t=5.94 s and t=12.16 s. High order schemes were employed for both time and space differentiation, respectively 3^{rd} order RK scheme and 3^{rd} order Quick scheme [8]. The 2^{nd} order central scheme which as known is more adequate for LES could also be applied for this test case, albeit showing some instability at certain events. The overall

simulation time for MPI parallel execution was 80 H on a 128 processors supercomputer. The convergence criteria set for pressure was (maximum) 0.5e-3 for each time step. Mesh sensitivity study has revealed that the 2.5 million cell grid provides virtually the same results as a 4 million cell mesh (results not shown here). No error analysis was conducted in the sense of VUQ.

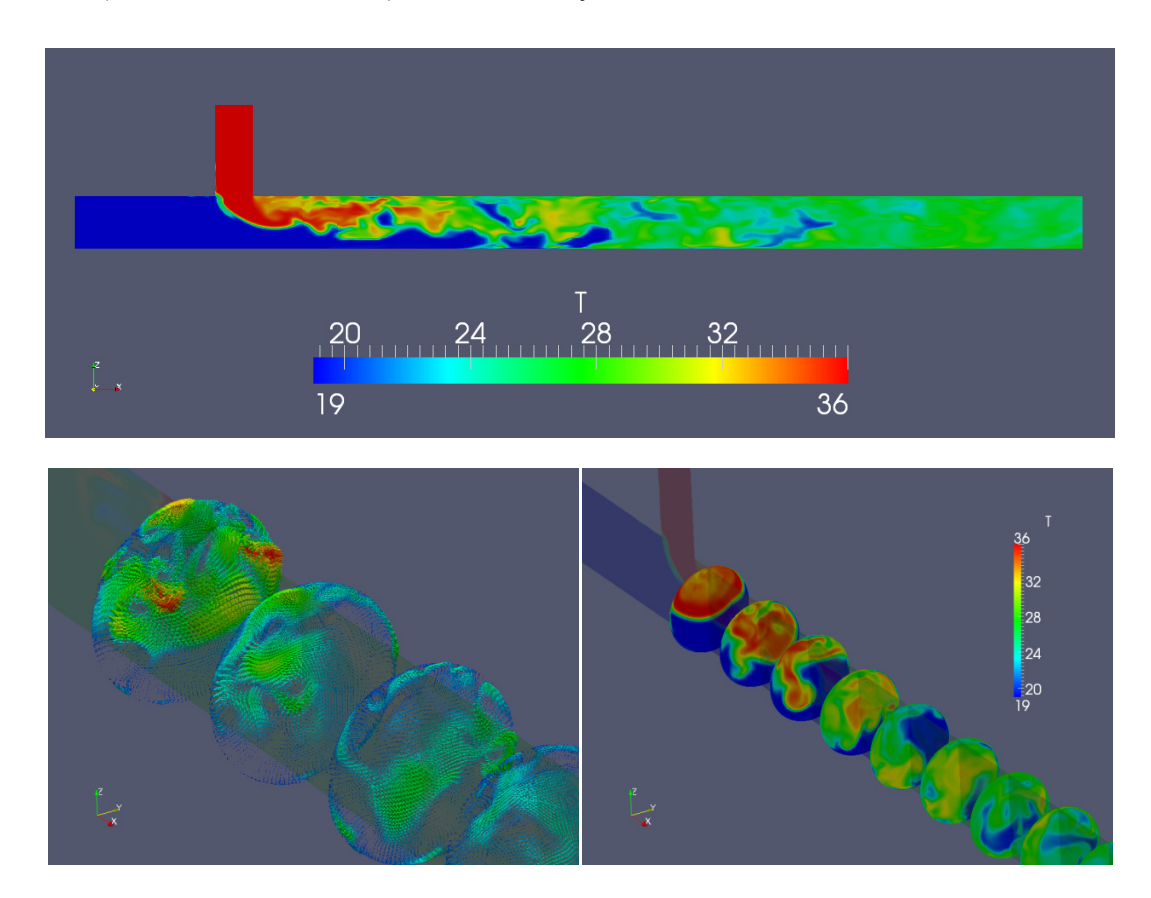


Figure 3: Instantaneous thermal flow results

3.3 Transient results

Qualitative flow features are depicted in Fig. 3, showing the heat contours (upper panel) and the flow structures developing in the flow direction. The upper panel suggests already that as was to be expected the location of the maximum thermal loads is on the upper pipe side immediately downstream the junction (1D). The heat diffuses rather fast downstream at about 6D from the junction. The secondary flow motion shown in the second panel and colored with temperature contours suggests a strong turbulence activity in the pipe. The most vigorous secondary vortices are precisely located close to the region of maximum thermal stripping on the pipe.

3.4 Time-average results

Time averaged results are shown in Figs. 4-6, including the measurement data for comparison as well. The agreement with the experiment is very good, both for the velocity and the stresses, at various locations of the pipe. A slight discrepancy is observed in the core pipe flow region. The reasons for this difference are the averaging time; these discrepancies were even worse for the first results shown at the CFD4NRS workshop held in Washington (after 100.000 time steps).

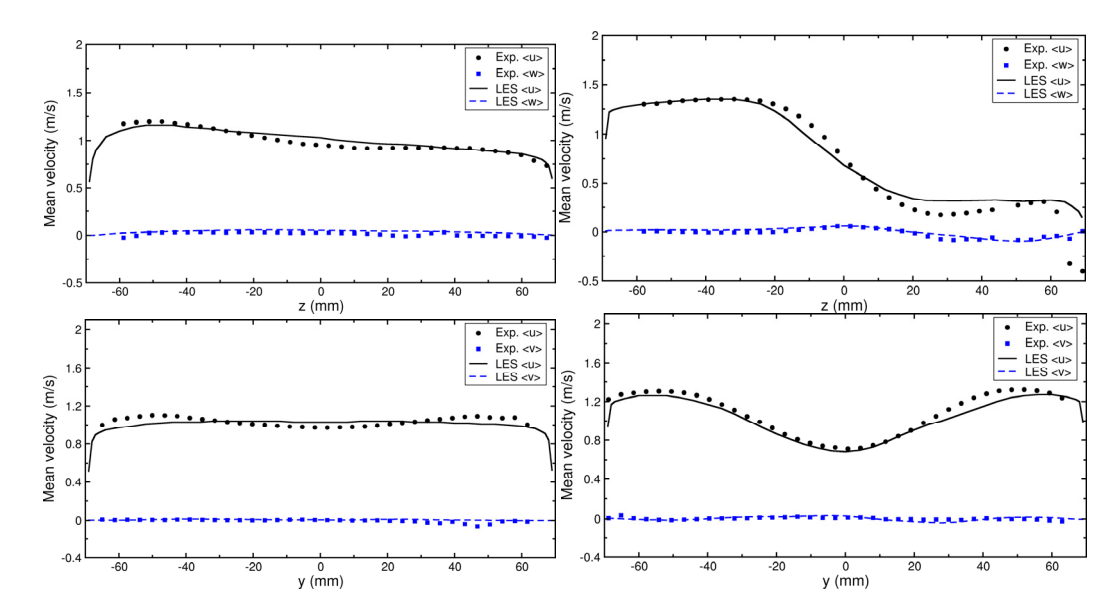


Figure 4: Time average velocity profiles at various locations of the pipe

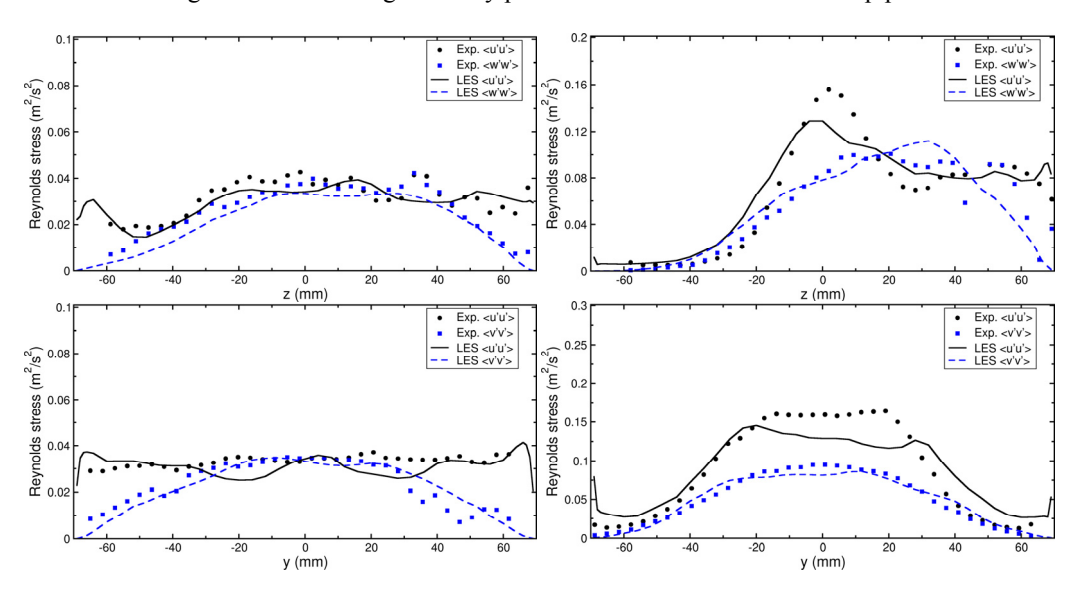


Figure 5: Reynolds stresses profiles at various locations of the pipe

The results shown below were obtained after 150.000 time steps, 50.000 extra time steps compared to the results discussed in Washington. The same is true for the temperature (mean and RMS) profiles plotted in Fig. 6 below. The agreement with the data is simply excellent.

4. Turbulent flow in a heated closed channel

4.1 Problem setup

The DSM model of TransAT is used to predict a turbulent channel flow differentially heated from both walls (290 & 310 K). Statistically converged turbulent fields were generated for Pr = 0.1, 1.0 & 10, at a shear Reynolds number $Re_{\tau} = u_{\tau}h/2\mu = 200$ (based on the half channel height).

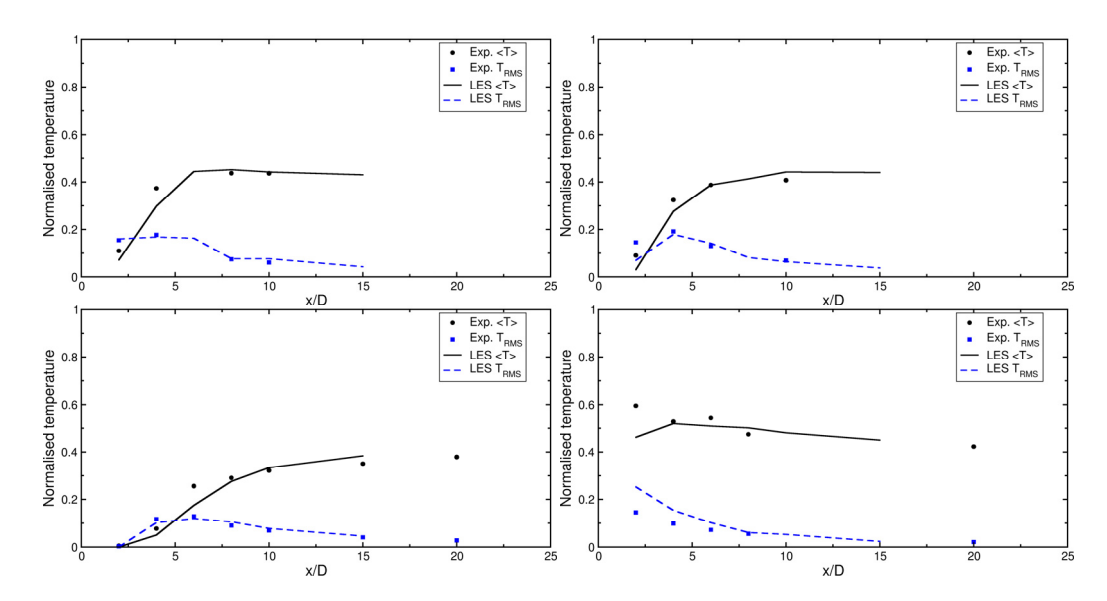


Figure 6: Time average and RMS temperature profiles at various locations of the pipe

The computational grid is rather coarse: 64^3 for Pr = 0.1 and 1.0, and 64x128x64 for Pr = 10; the latter one requires indeed higher cross-flow resolution to capture thermal structures. The numerical strategy employed is the same as for the former case. Comparisons with available DNS data at $Re_\tau = 150$, 171 were performed. The wall-neighboring cell was set such the resulting value of y^+ falls within the range where a damping function is not unity in order to accommodate the asymptotic behavior of turbulence: $v_t \sim z^3$. Periodic boundary conditions were set at the streamwise and spanwise directions of the domain. An adaptive time-stepping strategy (using explicit scheme) has been employed, ensuring that CFL < 0.3. The flow reaches a steady state after about 50.000 time steps, after which time averaging of the flow has been performed, typically for another 100.000 time steps. Typical simulation time for the 64^3 grid using 36 parallel processors on the DOE supercomputer 'Jaguar' was 5H for the 100.000 time steps, against 48.5H on a Quadcore local PC. The mesh sensitivity study was inspired from the various past investigations of the same flow for the same range of Reynolds number. No error analysis was conducted in the sense of VUQ.

4.2 Instantaneous results

The generated turbulence is well depicted in Fig. 7, showing instantaneous cross-flow velocity and thermal fields for Pr = 1. Turbulent structures formed near the wall are clearly carrying the heat to the outer core flow region. The results thermal fields shown in Fig. 8 suggest that structures are quite different, with a marked distinction for Pr=0.1, the case with the fastest scalar diffusion and the thickest thermal boundary layer. The Pr=10 results reflect clearly another structure of the thermal boundary layer, a fact amply corroborated by the time averaged heat profiles discussed in Subsection 4.3. Figure 9 comparing the resulting instantaneous 2D-plane SGS turbulent Prandtl number suggests that the model predicts indeed values deviating substantially from unity, falling within the range $0.01 < Pr_t < 10$ independently from the value of Pr. Note that that the DMS model may produce overshoots (up to $Pr_t < 100$).

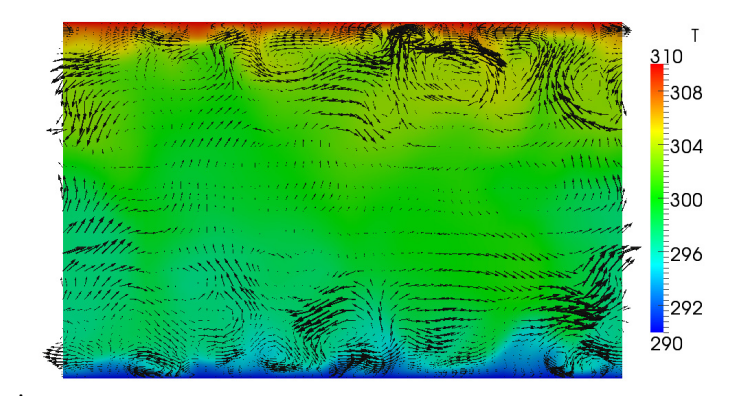


Figure 7: Instantaneous cross-flow velocity and thermal fields for Pr = 1

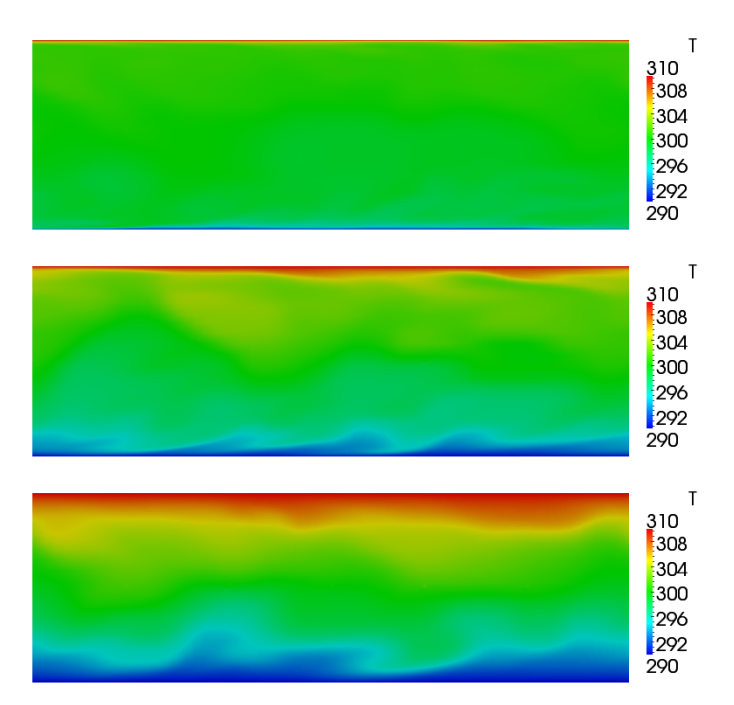


Figure 8: Instantaneous thermal fields in the flow direction for Pr = 0.1, 1 & 10

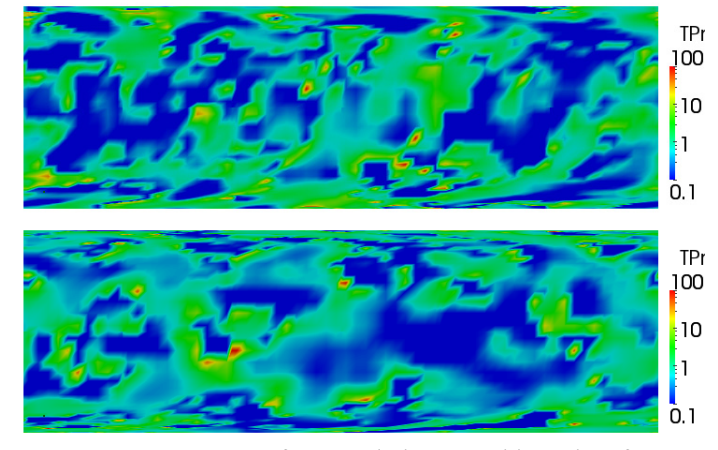


Figure 9: Instantaneous contours of SGS turbulent Prandtl number, for Pr = 0.1 & 10

4.3 Time-average results

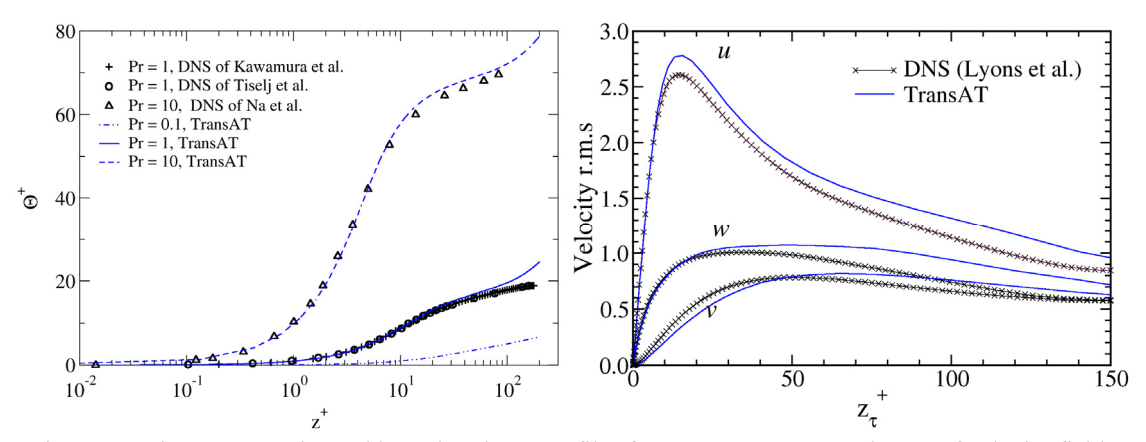


Figure 10: Time average thermal boundary layer profiles for Pr = 0.1, 1 & 10 and r.m.s of velocity field

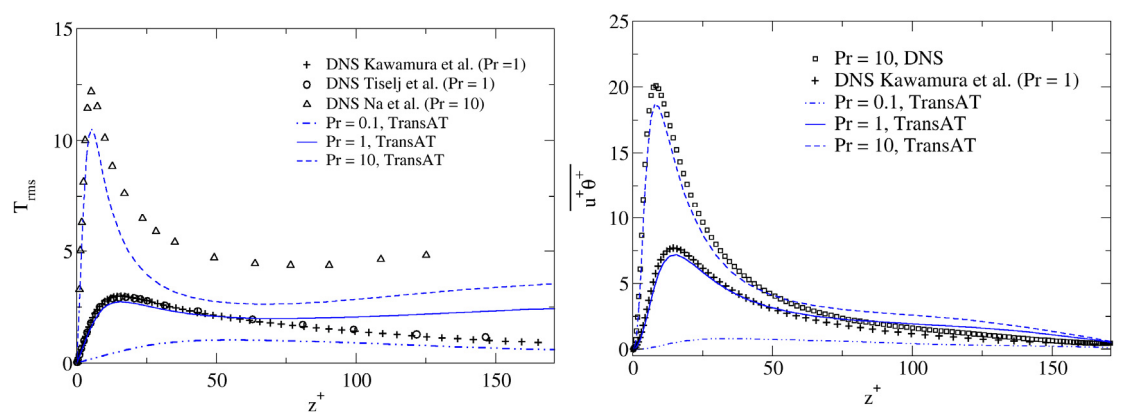


Figure 11: RMS of temperature fields and averaged heat fluxes for Pr = 0.1, 1 & 10

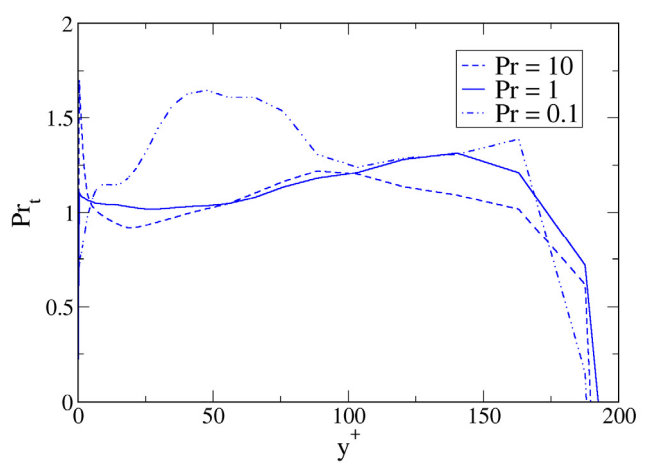


Figure 12: Time average turbulent Prandtl number for for Pr = 0.1, 1 & 10

Figure 10 depicts the resulting time averaged thermal profiles for Pr = 0.1, 1 & 10 and the r.m.s of the velocity field field. The LES data overall compare very well with the various DNS results despite the fact that the grid is actually rather coarse, in particular for the Pr = 10 case; the DNS of Na et al. [15] used for comparison for that Pr = 10 required actually a much finer grid resolution: 128^3 . The slight difference between the present r.m.s. results and those of Lyons et al. [16] are due to the difference in Pr Ret; 200 against 150. The left panel indicates clearly that the thermal boundary layer thins with increasing Pr.

Figure 11 compares the r.m.s. of temperature and related heat fluxes obtained with the DSM model with existing DNS data [13-17] for various Pr numbers. Overall the comparison between LES and DNS is quite satisfactory, in particular for Pr=1. The fluctuating temperature field is underpredicted in the core flow zone for Pr =10, because of the coarse grid resolution employed in this case. The right panel shows that the LES predicts very well the DNS data for both Pr =1 and 10; The DNS data are due to Lakehal et al. [17], who also used a 64x128x64 grid, coarser than Kawamura's DNS campaign. While there is no DNS data available for comparison for Pr=0.1, we could clearly see that thermal field in that case behaves almost like a laminar flow, with very little fluctuations and very weak heat flux, unlike the Pr =1 and 10 cases, where for the peak of r.m.s fluctuations reaches 12.5 in DNS. It might be that modeling the SGS thermal effects in LES for Pr <<1 convective flows is actually unnecessary; the supergrid effects are sufficient to predict the flow behavior.

Once the space-and-time averaged data base has been extracted, we now move to exploring the results in terms of model upscaling. The interest is clearly on the turbulent Prandtl number, determined here using its exact definition as the ratio of space-and-time averaged shear stress to heat flux. These averaged profiles shown in Fig. 12 provide an indication of the distribution up to $y+\sim100$; beyond that, near the channel centerline, the definition becomes ill posed. The model predicts values within the expected range $0.7 < Pr_t < 1.75$. Near the wall, the behavior is different from the outer core flow, depending on Pr: while for Pr =1 the turbulent counterpart oscillates around unity, too, Pr_t values tend to decrease from the wall for Pr=10 and increase from the wall for Pr=0.1. Whether these results could be used as a coarse-grained model for RANS applications in unclear, but worth trying.

In the light of these findings, extending the dynamic SGS model for convective heat transfer problems with non-unity Pr number flows seems to be promising, if not to be employed for practical problems, it will have the merit to help calibrate simple analytical correlations.

5. Conclusions

LES of turbulent thermal flow fields has been shown to yield accurate results for a complex flow in T-junction. Presumably such quality results would have been very difficult to obtain using a RANS approach. The thermal field in the T-junction was computed using a fixed turbulent Prandtl number. The results of this first part helped validate the LES approach in TransAT.

A variable turbulent Prandtl number sub-grid scale model using the dynamic approach was implemented in TransAT to advance the modeling of the turbulent thermal field. LES of a flow between parallel plates was performed for three different molecular Prandtl numbers using the variable Prt model and with a constant specified Pr_t =1. Time-averaged turbulent Prandtl number

variation was obtained that shows a peak near the wall, with values as high as 1.75. Away from the wall a slow variation between 0.7 and 1.0 was observed. A monotonic behavior of the turbulent Prandtl number with respect to the molecular Prandtl number as stipulated by various models was not observed. Turbulent thermal statistics were calculated and compared to DNS data

Overall the LES results match quite well the DNS, with an over-prediction of fluctuating thermal field for the high Pr case typically attributed to under-resolution in LES. All other quantities predicted with LES are comparable to DNS, despite the coarse grids employed. The study shows that modeling the SGS thermal effects in LES for Pr <<1 convective flows is probably unnecessary; the supergrid effects are sufficient to predict the flow behavior. But further detailed study is required over a broader range of parameters to clarify the effect of variable Pr_t .

Acknowledgements

This research is financially supported by the THINS research project (2010-2013) of the Euratom 7th Framework Programme. The simulations were run on the DOE Supercomputer Jaguar, within the Scalability Analysis Task performed within the DOE CASL project coordinated by Doug Kothe ORNL (MNM Workpackage led by Robert Lowrie, LANL).

References

- [1] D. K. Lilly, Phys. Fluids A, 4, 633-635, 1992
- [2] T. Schulenberg, R. Stieglitz, R, Nucl. Eng. Design, 240, 2077–2087, 2010
- [3] J. Licht, M. Anderson, M. Corradini, J. Heat Transfer, 131-7, 072502, 2009
- [4] M. Jischa, H. Rieke, Int. J. Heat & Mass Transfer, 22, 1547, 1979.
- [5] W. M. Kays, J. Heat Transfer, 116, 284-295, 1994
- [6] B. Launder, J. Heat Transfer, 110, 1112-1128, 1998
- [7] K. Hanjàlic, Ann. Rev. Fluid Mech., 34, 321-347, 2004
- [8] TransAT User Manual, 2011, ASCOMP Switzerland
- [9] P. Moin, K. Squires, W. Cabot, S. Lee, Phys. Fluids, 3(11), 2746-2757, 1991
- [10] S-H. Peng, L. Davidson, Int. J. Heat & Fluid Flow, 22, 323-331, 2001
- [11] J. Westin, P. Veber, L. Andersson, C. Mannetje, U. Andersson, J. Eriksson, M. Hendriksson,
- F. Alavyoon, C. Andersson, ICONE-16, Paper No. 48731, 1-11, 2008
- [12] F. Nicoud, F. Ducros, Flow, Turbulence and Combustion, 62, 183-200, 1999
- [13] H. Kawamura, K. Ohsake, H. Abe, K. Yamamoto, Int. J. Heat Fluid Flow, 20, 482, 1998
- [14] I. Tiselj, R. Bergant, B. Mavko, I. Bajsic, G. Hetsroni, J. Heat Transfer, 123, 849, 2001
- [15] Y. Na, D. V. Papavassiliou, T. J. Hanratty, Int. J. Heat Fluid Flow, 20, 187, 1999
- [16] S. L. Lyons, T. J. Hanratty, J. B. McLaughlin, Int. J. Numer. Methods Fluids, 13, 999, 1991
- [17] D. Lakehal, M. Fulgosi, G. Yadigaroglu & S. Banerjee, J. Heat Transfer, 125, 1129, 2003